Article

J. Mex. Chem. Soc. **2008**, *51(4)*, 36-46

ISSN 1870-249X

Mechanism and Kinetics of the OH• Radical Reaction with Formaldehyde Bound to an $Si(OH)_4$ Monomer

Cristina Iuga[1], Rodolfo Esquivel Olea[1], and Annik Vivier-Bunge[1]

[1]Departamento de Química, Universidad Autónoma Metropolitana, Iztapalapa, México, D.F., México. Email: annik@xanum.uam.mx

Recibido el 3 de octubre del 2007; aceptado el 25 de enero del 2008

Abstract. In this work, quantum chemical methods are used to study the reaction of OH• radicals with formaldehyde bound to the $Si(OH)_4$ monomer, as a model for silica mineral aerosols. The potential energy surfaces for the formaldehyde interaction with the surface model have been carefully spanned, and minima and maxima were evaluated. Both the H-abstraction and OH-addition paths are shown to be complex reactions, which involve the formation of a reactant complex in the entrance channel and a product complex in the exit channel. In the main reaction channel, formaldehyde binds to the silanol groups and then reacts with OH free radicals to form a water molecule and a bound formyl radical. We show that the rate constant for the H-abstraction reaction is an order of magnitude smaller when formaldehyde is bound to $Si(OH)_4$ than in the gas phase, while the rate constant for the addition reaction is still about five orders of magnitude smaller. Thus, the branching ratio between abstraction and addition is not significantly altered in the presence of the silicate surface model.
Key words: Mineral aerosols, radical reactions, silica surface model, formaldehyde, OH radicals, rate constants

Resumen. En este trabajo, se utilizan métodos de la química cuántica para estudiar la reacción de radicales OH con formaldehído adsorbido sobre $Si(OH)_4$, como modelo de superficie para representar aerosoles de silicatos minerales. Se evalúan mínimos y máximos en las superficies de energía potencial para la interacción de formaldehído con la superficie modelo. Las reacciones correspondientes a la abstracción de hidrógeno y a la adición del radical OH son complejas, y ambas involucran la formación de un complejo pre-reactivo en el inicio del camino de reacción, así como un complejo de productos después del estado de transición. En la reacción más importante, que corresponde a la abstracción de un hidrógeno del formaldehído, éste se une a grupos silanol de la superficie modelo, y posteriormente reacciona con radicales libres OH para formar una molécula de agua libre y un radical formilo anclado a la superficie. Se muestra que la constante de velocidad de la abstracción de hidrógeno es un orden de magnitud menor que para la misma reacción en fase gas, mientras que la de la adición es aproximadamente cinco órdenes de magnitud más pequeña. De acuerdo con este modelo, la proporción entre abstracción y adición no se altera significativamente en presencia de un aerosol mineral.
Palabras clave: Aerosoles minerales, reacciones radicalarias, superficie modelo de silicatos, formaldehído, radicales OH, constantes de velocidad.

Introduction

A major natural component of atmospheric aerosol is mineral dust, which enters the troposphere from dust storms in arid and semiarid regions. Mineral aerosols are fine particles of crustal origin that are generated by wind erosion, and that consist mostly of silica and silicate minerals. The potentially reactive surface of mineral aerosols may be a significant sink for many volatile organic compounds in the atmosphere and consequently it could influence the global photooxidant budget. Laboratory studies, together with field observations and modeling calculations, have clearly demonstrated the importance of heterogeneous processes in the atmosphere. The subject has recently been reviewed by Usher *et al.* [1] Some articles have tried to quantify the effect of dust on tropospheric chemistry. Dentener *et al.* [2] calculated that ozone concentration would decrease because O_3 production decreased (N_2O_5 and HO_2 radicals are taken up on dust) and also because the O_3 molecules were themselves taken up on dust. Bian and Zender [3] found that, on a global average, O_3 decreases by 0.7%, OH decreases by 11.1%, and HO_2 decreases by 3.5 % when dust is added to the atmosphere. As discussed by Ravishankara [4], the ability for predicting accurately the composition of the troposphere will depend on advances in understanding the role of particulate matter and the extent to which heterogeneous reactions on solids as well as multiphase reactions in liquid droplets contribute to the chemistry. Thus, the heterogeneous chemistry of trace atmospheric gases on solid-phase particles in the troposphere is a field of great interest.

The primordial role of OH radicals in the oxidative transformation of volatile organic compounds and other pollutants in the troposphere is well accepted. However, the catalytic loss processes of atmospheric pollutants in the presence of OH radicals and aerosols may affect the chemical reactions of OH radicals with adsorbed pollutants [5, 6].

Formaldehyde is one of the most prevalent carbonyl compounds in the Earth's atmosphere; it is an important component of the polluted troposphere and it is a precursor of HO*x* radicals. Thus, any heterogeneous interactions that formaldehyde may have with aerosols could potentially affect HO*x* levels, especially if the former is removed from the troposphere. The heterogeneous uptake of formaldehyde on SiO_2 has recently been examined [7].

Formaldehyde may, in principle, react with an OH radical through two reaction paths: the abstraction of a hydrogen atom and the subsequent formation of a water molecule and a formyl radical (Eq. 1); or, the addition of one OH radical to the C=O double bond, with formation of the $H_2C(OH)O$• alkoxy radical

(Eq. 2). In the gas phase at room temperature, the abstraction reaction is favoured.

Abstraction:

$$CH_2O + \bullet OH \rightarrow CHO\bullet + H_2O \quad (1)$$

Addition:

$$CH_2O + \bullet OH \rightarrow \bullet CH_2O(OH) \quad (2)$$

The rate constant for reaction of OH with formaldehyde is virtually independent of temperature in the region of atmospheric relevance, while the higher aldehydes all show a slight negative temperature dependence [8, 9,10]. The experimentally determined Arrhenius parameters [11, 12] indicate that the activation energy barrier is very small, close to zero. Ab initio calculations indicate that the reaction channel involving addition to the carbonyl group has a significantly higher activation energy than the elimination pathway [10,13,14]. However, if the formaldehyde molecule were anchored to a clay surface, the branching ratio between abstraction and addition could be altered.

The rigid tetrahedron SiO_4 is the building block of all siliceous materials, from zeolites to quartz and amorphous silica. Clay minerals, or phyllosilicates, are formed by sheets of SiO_4 tetrahedrons joined to a sheet of Al oxide octahedrons (Figure 1). The ideal surface of a phyllosilicate is characterized by the presence of a large number of siloxane Si-O-Si bridges, forming hexagonal rings. However, a natural clay surface presents many structural defects and fractures, and its chemical properties are largely due to the presence of active sites on the surface, which are mainly acid sites: Brönsted sites, associated to aluminol and silanol groups, and Lewis sites, such as in four-coordinated Al. Phyllosilicates have large specific surfaces and catalytic properties. Therefore, their presence in aerosols can be expected to play an important role in the heterogeneous chemistry of the troposphere.

The different types of OH surface groups are schematically represented in Figure 2. In addition to isolated hydroxyl groups, at the surface of outgassed amorphous silica, geminal hydroxyls (i.e., two hydroxyls sitting on the same Si atom) are known to occur. The evidence for geminal silanols comes from NMR spectra [15, 16], which show distinct signals for geminal and isolated hydroxyls [17, 18, 19, 20]. Peak intensities suggest that the population of geminal hydroxyls constitutes a substantial fraction (up to 30%) of isolated hydroxyls. At the surface of crystalline specimens, the presence of geminal species could be even more substantial. Therefore, any difference in the adsorptive properties between isolated and geminal hydroxyl groups may affect the overall behavior of silica. However, as isolated and geminal species present O-H stretching modes that are indistinguishable in the IR, [21, 22] it is not easy to bring into evidence their differences. These have been often hypothesized, in particular towards water, because of the presence, in geminal species, of a potentially active bifunctionality [23, 24, 25]. The review of Heanry *et al.* [26] gives a detailed account of the Si-O bond in these systems.

Within the quantum mechanical treatment, different small clusters have been used in the literature to model silicate surfaces. The basic premise behind this approach is that reactions and adsorption are local phenomena, primarily affected by the nearby surface structure. The advantage of the cluster approach is that the active site is described explicitly by the interactions between the local molecular orbitals of the adsorbate and the adsorbent. On the other hand, the disadvantage is the incomplete representation of the electronic system provided by the small size and the discrete nature of the cluster employed. However, by carefully optimizing the adsorbate-cluster interactions, the lowest energy structures and electronic states can be calculated and used to predict energetic data at high levels of theory and with large basis sets, thus yielding accurate energetic results.

Sauer and co-workers performed an exhaustive revision of quantum mechanical models used to study molecule-solid interactions. Molecular Van der Waals complexes between adsorbed molecules and surfaces have been studied, and adsorption energies have been reproduced for a large number of compounds [27]. The reactivity of some unimolecular reactions of adsorbed species was determined by Usher *et al.* [1] The adsorption of methanol, formaldehyde and formic acid on Si surfaces was studied by Lu *et al.* [28] using DFT methods and ONIOM calculations on an Si_9H_{12} cluster model. More recently, the study of the interaction between isolated silica hydroxyls and small molecules has been carried out using *ab initio* quantum chemistry methods, mimicking the surface species by means of the silanol molecule H_3SiOH [29]. One paper was specifically devoted to the interaction between H_3SiOH

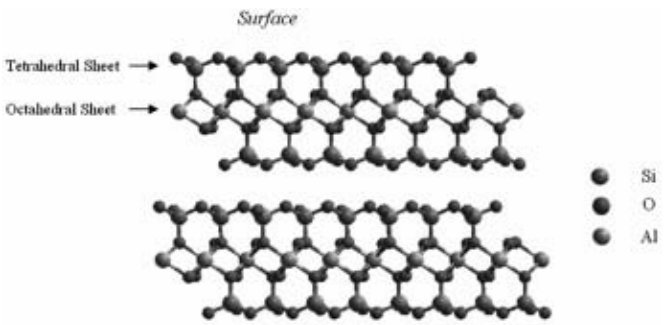

Fig. 1. Typical structure of a 1:1 layered phyllosilicate.

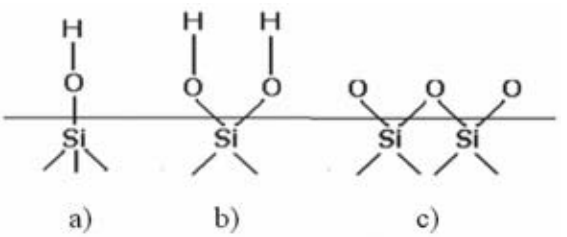

Fig. 2. Surface active sites at the silica surface; a) isolated silanol group, b) geminal silanol groups, and c) siloxane bridge.

and formaldehyde [30]. IR data at 170 K of the interaction of CH_2O on amorphous silica were also reported [31], and the conclusion was that the computed harmonic vibrational frequencies were in fair agreement with the experimental results.

Orthosilicic acid $Si(OH)_4$ in various conformations, alone and in interaction with water, has been studied, using ab initio methods, by Sauer and Schrader [32] at low levels of treatment (STO-3G, 3-21G, 4-31G basis sets). Indications from these simple calculations are that the stretching modes of geminal and isolated species are indeed indistinguishable, and that the bifunctional nature of the former does not impart any particular affinity for the water molecule. Two conformations of orthosilicic acid have been studied ab-initio in interaction with a water molecule [33].

The minimal cluster for the description of an isolated hydroxyl group at the silica surface is the silanol molecule H_3-SiOH [34, 35]. The overall evidence [36] is that the OH group of the silanol molecule is probably somewhat less acidic than a real hydroxyl group of silica, but nonetheless it serves quite well as a model [37]. In the same line, the silanediol molecule $H_2Si(OH)_2$ may be assumed as the simplest cluster mimicking geminal SiOH species. Alternatively, orthosilicic acid $Si(OH)_4$ may be considered as a model for both the isolated and geminal types of hydroxyls, by considering one and two silanol groups, respectively, as active centers, and the remaining ones just as cluster terminators. The use of these clusters has been well validated [38, 39].

From a theoretical point of view, two initial considerations have to be made: first the choice of the adsorption site model, relating to chemical structural aspects, and second the technical questions of the computational approach and accuracy. In this work, the mechanism of both the H-abstraction and addition channels of the formaldehyde + OH reaction will be studied, with formaldehyde attached to an $Si(OH)_4$ orthosilicic acid molecule. An exhaustive search of optimized structures for bounded formaldehyde and stationary points along the reaction coordinates will be performed. With the corresponding partition functions, the effective rate constants will then be calculated, using classical transition-state theory and the proposed mechanisms. The results will be compared with the experimental data in the gas phase. Our aim is to investigate the effect that the presence of orthosilicic acid has on the reaction, and to determine whether or not the attached formaldehyde reacts faster with OH radicals than when it is free. To the best of our knowledge, this is the first theoretical study of a reaction between an adsorbed molecule and a free radical.

Computational Methodology

Ab initio quantum chemical calculations were performed using the density functional theory (DFT) method with the hybrid functional BHandHLYP/6-311G** [40, 41] as implemented in the Gaussian03 program package [42]. The method was chosen because excellent results have been obtained with this functional in other hydrogen abstraction reactions in the gas phase [43, 44]. All geometries were fully optimized at this level using the Berny analytical gradient method. No geometry constraints were applied on the surface and reactants atoms. The unrestricted approximation was used for radicals. Oftentimes, difficulties were encountered in the search for the optimized structures, with respect to convergence of the SCF. This problem was solved by using a quadratic convergence algorithm (QC), which is an option based on the Newton-Raphson method. Although it is quite efficient, it requires a large number of iterations, and consequently a significant amount of CPU calculation time. We also employed the IOP(1/8=1) option, in order to reduce the atomic displacements, both in distances and in angles, during geometry optimization. Normal mode analyses were carried out at the same level to confirm the nature of the stationary points, finding only positive eigenvalues for minima and one negative eigenvalue (imaginary frequency) for transition states. It was verified that the motion along the reaction coordinate corresponds to the expected transition vector. Corrections for zero-point energy (ZPE) (residual vibrational energy at 0 K) were taken from the force constant analysis and added to the total energies.

The relevance of the Basis Set Superposition Error (BSSE) has been well established from a theoretical point of view [45, 46]. However, there has been a wide controversy on the reliability of the results produced by adding the counterpoise correction (CP) [47, 48]. It has been pointed out that CP often over-correct the results due to the fact that the BSSE and the basis set convergence error are often of opposite signs [49]. CBS schemes, on the other hand, correct both kinds of errors, while the Counterpoise approach corrects only the first one, leading to artificially high energies. For most systems of chemical interest the CBS extrapolation is computationally unaffordable. Fortunately this is not the case for the quantum chemical treatment of the particular systems treated in this work. Accordingly, CBS-QB3 calculations were also performed, as implemented in Gaussian, i.e. with geometry optimizations and frequency calculations at the B3LYP/CBSB7 level of theory, for the main reaction channel.

In order to study the reaction of an OH radical with a volatile organic compound adsorbed on $Si(OH)_4$ as a model surface for a mineral dust aerosol, we have chosen the reaction of a formaldehyde molecule with an OH radical. On the one hand, the formaldehyde is a very reactive polar molecule that is easily adsorbed on surfaces, and on the other hand, many theoretical and experimental data are available for the corresponding gas phase reaction.

The mechanism is well accepted. It involves two steps: at first, a fast pre-equilibrium between the reactants (R) and the pre-reactive complex (RC) is established, followed by an internal rearrangement leading to the elimination of a water molecule.

$$\text{Step 1: } RHC{=}O + OH\bullet \underset{k_{-1}}{\overset{k_1}{\rightleftharpoons}} [RHC{=}O \text{ ----} HO\bullet] \qquad (3)$$

$$\text{Step 2: } [RHC{=}O \text{ —— } HO\bullet] \xrightarrow{k_2} RC{=}O\bullet + H_2O \qquad (4)$$

In this work, the calculated rate constant and the corresponding kinetic parameters, are obtained using conventional Transition State Theory (CTST) [50, 51] implemented in the Rate 1.1 program [52] and the reaction mechanism proposed above (Eqs. 3 aad 4). According to this mechanism, if k_1 and k_{-1} are the forward and reverse rate constants for the first step and k_2 corresponds to the second step, a steady-state analysis leads to a rate coefficient for each overall reaction channel that can be written as:

$$k = \frac{k_1 k_2}{k_{-1} + k_2}.$$

Even though the energy barrier for k_{-1} is about the same size as that for k_2, the entropy change is much larger in the reverse reaction than in the formation of the products. Thus, following a hypothesis first proposed by Singleton and Cvetanovic [53], k_2 is expected to be much smaller than k_{-1}. Based on this assumption, k can be rewritten as:

$$k = \frac{k_1 k_2}{k_{-1}} = \left(\frac{A_1 A_2}{A_{-1}}\right) \exp\left[-\left(E_1 + E_2 - E_{-1}\right)/RT\right],$$

where E_1 and E_{-1} are the Step 1 energy barriers corresponding to the forward and reverse directions, respectively, E_2 is the barrier for Step 2, and the A's are the partition functions. Since E_1 is zero, the net (or apparent) energy barrier for the overall reaction channel is:

$$E_a = E_2 - E_{-1} = \left(E_{TS} - E_{RC}\right) - \left(E_{RC} - E_R\right) = E_{TS} - E_R,$$

where E_{TS}, E_{RC} and E_R are the total energies of the transition state, the reactant complex and the reactants, respectively. Applying basic statistical thermodynamic principles the equilibrium constant (k_1/k_{-1}) of the fast pre-equilibrium between the reactants and the reactant complex may be obtained as:

$$K_{eq} = \frac{Q^{RC}}{Q^R} \exp\left[-\frac{E_{RC} - E_R}{RT}\right],$$

where Q^{RC} and Q^R represent the partition functions corresponding to the reactant complex and the isolated reactants, respectively.

Under sufficiently high-pressure conditions, such as normal conditions in the troposphere, an equilibrium distribution of reactants is maintained and the CTST formula can be applied [54] to calculate k_2:

$$k_2 = \kappa_2 \frac{k_B T}{h} \frac{Q^{TS}}{Q^{RC}} \exp\left[-\frac{E_{TS} - E_{RC}}{RT}\right],$$

where κ_2 is the tunneling factor, k_B and h are the Boltzmann and Planck constants, respectively, and Q^{TS} represents the transition state partition function. The energy differences include the ZPE corrections. The effective rate coefficient of each channel is then obtained as:

$$k_{ef} = \sigma K_{eq} k_2 = \sigma\kappa_2 \frac{k_B T}{h} \frac{Q^{TS}}{Q^R} \exp\left[-\frac{E_{TS} - E_R}{RT}\right],$$

where σ is the symmetry factor, which is related to the reaction path degeneracy. The symmetry factor is obtained by imaging all identical atoms to be labeled and by counting the number of different but equivalent arrangements that can be made by rotating the molecule [55].

Accurate rate constant calculations require the correct computation of the partition functions (Q). In this work, the hindered rotor approximation has been used to correct the Qs corresponding to internal rotations whose torsional barriers are smaller than 2.5 Kcal/mol. Direct inspection of the low-frequency modes of the studied stationary points indicates that several of them may correspond to hindered rotations. These modes have been identified and treated as hindered rotors instead of vibrations [56]. To make this correction, they were removed from the vibrational partition function of the corresponding species and replaced by the corresponding hindered rotor partition function.

We shall see that the rate constant for the gas phase reaction obtained with the methodology used in this work (see Table 4) agrees very well with the reported experimental values [57]. Therefore, one may assume that it is possible to use the same methodology to calculate reliable kinetic data for reactions on silicate surface models, for which experimental data are not available.

Results

The S_4 conformation of $Si(OH)_4$ is the global minimum energy for this molecule in the gas phase. Its optimized structure is presented in Figure 3. Full geometry optimization at the BHandHLYP/6-311g(d,p) level has been achieved, with all variables allowed to vary independently. The calculated Si-O bond is about 1.63 Å, in very good agreement with experimental data for clay minerals (1.62 Å for muscovite [58] and 1.64 Å for pyrophyllite [59]). The O-H distances are 0.95 Å.

Adsorption Complexes

Formaldehyde adsorbs on the model surface to form a complex. In principle, the formaldehyde molecule can bind in two different ways: i) the formaldehyde oxygen atom may be attracted to a silanol hydrogen atom while its hydrogen atom interacts with another silanol oxygen, forming the ADS1 adsorption complex (Figure 4.a), or ii) two formaldehyde hydrogen atoms may interact with the surface oxygens, giving

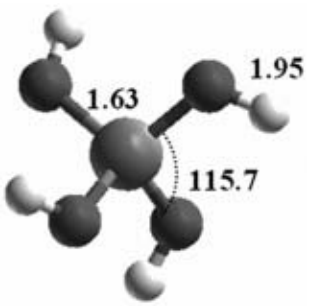

Fig. 3. Optimized structure of $Si(OH)_4$.

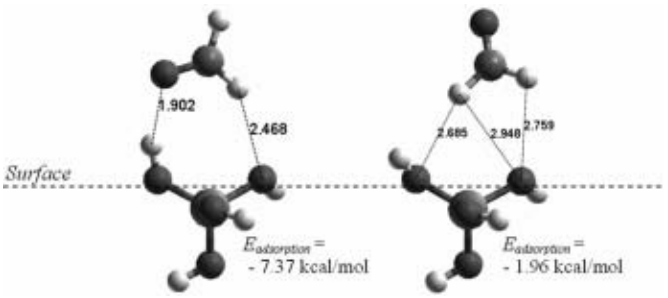

Fig. 4. Optimized structures of the adsorption complexes of formaldehyde on the $Si(OH)_4$.

rise to the ADS2 adsorption complexes (Figures 4.b). In this study, we consider both adsorption pathways.

The adsorption complexes have been fully optimized at the BHandHLYP/6-311g(d,p) level. In this process, the formaldehyde molecule is allowed to move freely until it reaches the optimum adsorption site. ADS1 and ADS2 complexes are obtained (Figure 4). In ADS1, the main interaction is a hydrogen bond, while in ADS2 both interactions are Van der Waals type weaker interactions. The geometry of the adsorbed CH_2O is slightly changed from that of free CH_2O, i. e., the C-H and C-O bonds are slightly larger.

The adsorption energy is defined as the difference between the total electronic energy of the surface-adsorbate complex and the sum of those of the isolated molecule and the model surface, including ZPE corrections:

$$E_{\text{adsorption}} = E_{\text{adsorption complex}} - (E_{\text{molecule}} + E_{\text{surface}}) + \Delta(\text{ZPE}).$$

The calculated adsorption energy values are negative, indicating that the adsorbate is stable. The ADS1 adsorption energy is -7.37 kcal/mol, while the one for ADS2 is more than 5 kcal/mol less negative, in agreement with the longer bond distance in the latter. The dipole moment of the ADS2 complex (3.74 Debyes) is larger than the one of the ADS1 complex (2.93 Debyes), because the formaldehyde C=O bond is highly polar and it is clearly oriented perpendicularly to the surface, while the compensation with the rest of the bonds is small. Surface hydroxyls play the role of weak hydrogen donors, while the adsorbed molecule assumes the role of the base.

Because of the chemical nature of the silanol groups, their vibrational properties can be studied by infrared spectroscopy. On highly dehydrated surfaces, a single, well-defined band due to the OH stretch is measured at about 3742 cm^{-1} on an otherwise featureless spectral region extending from 3730 to 2000 cm^{-1} [60]. It is possible to measure the shift of the silanol OH stretching frequency upon adsorption of the formaldehyde molecule from the gas phase. In that respect, it is now well-established that H-bonding interactions are a significant fraction of the forces between these silanol groups and formaldehyde [61].

In addition, the frequencies of the infrared absorptions calculated for formaldehyde adsorbed on SiO_4 at 1588, 1887, and 3030 cm^{-1} are close to those in the gas or liquid phase.[57], suggesting that this molecule is weakly adsorbed on SiO_4. The calculated silanol group stretching mode υ_{OH} in the ADS1 adsorption complex is 3858 cm^{-1}, and the anharmonic frequency shift $\Delta\upsilon_{OH}$ caused by the CH_2O adsorption on the silanol stretching mode has been computed to be -204 cm^{-1}. The calculated spectrum is shown in Figure 5 in cm^{-1}.

In the ADS2 adsorption complex no frequency shift is observed, because the formaldehyde hydrogen atoms interact with oxygen atoms of the silanol groups, thus the O-H vibrational motion is not affected.

Reaction mechanisms

First the H-abstraction and the OH•-addition stationary points in the gas phase reactions of formaldehyde with the OH• radical were recalculated at the BHandHLYP/6-311G** level, for comparison with the structures previously determined theoretically by Alvarez Idaboy et al. [13]. In addition to the pre-reactive complex obtained by these authors, another pre-reactive complex was identified, whose energy is 0.85 kcal/mol lower than the former, due to the stronger interaction between the hydroxyl oxygen and the formaldehyde hydrogen. To calculate

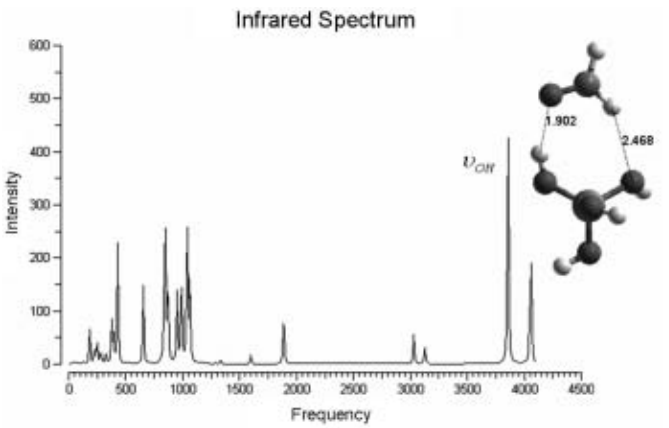

Fig. 5. ADS1 adsorption complex calculated infrared spectrum.

the relative energies of the reaction, we have used the new structure.

In the H-abstraction mechanism, the oxygen atom of the OH• radical approaches the hydrogen to be abstracted, as the energy increases to a maximum at the transition state (TS). A products complex (PC) is then obtained, which, in the next step, yields the final products. Our calculated activation energy barrier for the abstraction channel is 0.24 kcal/mol, which lies within the range of the available experimental results, which vary between +0.4 and -0.4 kcal/mol. [57] The optimized structures for the gas phase H-abstraction and OH•-addition channels are shown in Figures 6 and 9, respectively, for comparison purposes.

Next, the OH• reaction with the bound formaldehyde was investigated. The channels starting from ADS1 and ADS2 will be labeled M1 and M2, respectively. In the M1 H-abstraction mechanism, a water molecule is formed, and the formyl radical remains attached to the surface (Eq. 5), while in the M2 H-abstraction channel, the water molecule remains attached to the surface and the formyl radical is free (Eq. 6). Thus the overall reactions can be written as:

M1 H-abstraction:

$$\mathbf{ADS1} + OH\bullet \rightarrow \mathbf{S} \bullet\bullet\bullet\bullet HCO\bullet + H_2O \qquad (5)$$

M2 H-abstraction:

$$\mathbf{ADS2} + OH\bullet \rightarrow \mathbf{S} \bullet\bullet\bullet\bullet H_2O + HCO\bullet \qquad (6)$$

where **S** stands for the surface.

For the addition mechanisms, the oxygen atom approaches the carbon atom of the formaldehyde from above and a surface bound adduct is formed:

M1 OH-addition:

$$\mathbf{ADS1} + OH\bullet \rightarrow \mathbf{S} \bullet\bullet\bullet\bullet \bullet CH_2O(OH) \qquad (7)$$

M2 OH-addition:

$$\mathbf{ADS2} + OH\bullet \rightarrow \mathbf{S} \bullet\bullet\bullet\bullet \bullet CH_2O(OH) \qquad (8)$$

All the stationary points will be described next.

Pre-reactive Complexes

In the pre-reactive complexes, the approach of the OH• radical to the adsorbed formaldehyde molecule is guided mainly by the Coulomb interaction between the positively charged hydrogen atom of the OH• radical and a lone pair of the formaldehyde oxygen atom. The interactions determine the shape and stability of the pre-reactive complexes as well as the rest of the reaction. Different pre-reactive complexes are obtained for the M1 and M2 channels, but in all cases, the structure of the adsorption ADS1 and ADS2 complexes remains almost unchanged in the process. Both are more stable than in the gas phase, with E_{-1} stabilization energies of -4.96 and -5.32 kcal/mol, respectively. They are shown in Figures 7.a and 8.a. Relevant geometrical parameters have been indicated on the figures. The non-bonding O...H distances between the OH• radical and the adsorbed formaldehyde are given in Table 1. Atoms belonging to the OH• radical are indicated by the *oh* subscript, while those in formaldehyde are denoted by an *f* subscript. We note that the most important interaction is the one between the OH• hydrogen atom H_{oh} and the formaldehyde O atom (O_f).

The pre-reactive complexes are common to both abstraction and addition channels. These will be described next in detail.

H-abstraction Mechanism

In the H-abstraction channel, the OH• radical approaches the adsorption complex from above, in order to remove the hydrogen atom that is not surface-bound. At this point it is necessary to distinguish between the M1 and M2 mechanisms.

In the M1 H-abstraction mechanism, the transition state that is obtained resembles the one in the gas phase reaction, because the hydrogen atom that is to be abstracted is free of surface interactions (Figure 7.b). Inspection of the vibrational mode corresponding to the imaginary frequency of the transition state indicates that this vibration is essentially the motion of a light atom (H) between two fixed heavier atoms (C and O). There is little heavy atom motion as the system moves along the reaction path. The product complex presents a hydrogen bonds between the water molecule and the oxygen atom of the formyl radical and it is only about 2 kcal/mol more stable than the corresponding separated products. The resulting effective activation energy, $E_a^{eff} = E_{TS} - E_R$ is slightly larger (0.95 kcal/mol) than in the gas phase (0.24 kcak/mol), because the transition state occurs considerably later. The $O_{oh}\ldots H_f$ distance between the oxygen atom of the OH• radical and the hydrogen atom which is abstracted is 1.35 Å, as compared to 1.38 Å for the gas phase, indicating that the H_f atom in the M1 channel is less tightly bound. It is important to note that the energy barrier of the second step, $E_2 = E_{TS} - E_{RC}$, is also larger

Table 1. Non-bonding O...H distances (in Å) in the pre-reactive complexes.

Mechanism	d $H_{oh}\ldots O_f$	d $O_{oh}\ldots H_f$
Gas phase	1.96	2.72
M1	1.98	2.67
M2	1.91	2.80

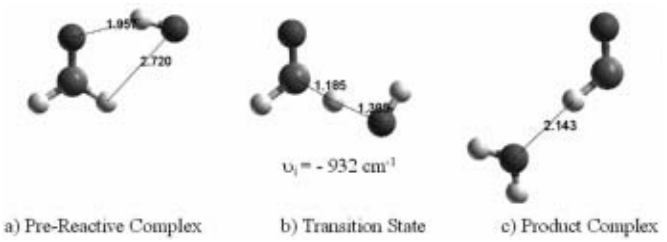

Fig. 6. Optimized structures in the gas phase H-abstraction reaction (BhandHLYP/6-311g(d,p)).

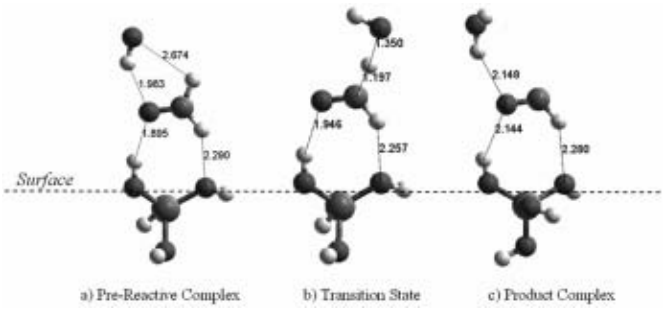

Fig. 7. Optimized structures in the M1 H-abstraction reaction on $Si(OH)_4$ cluster (BhandHLYP/6-311g(d,p)).

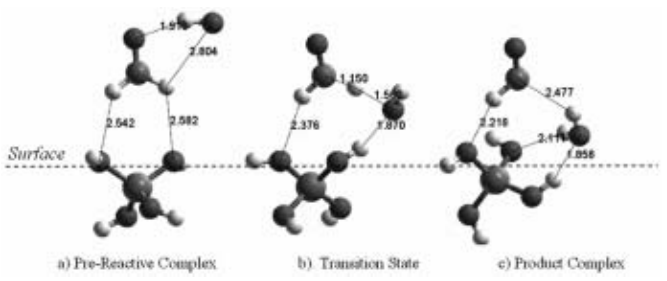

Fig. 8. Optimized structures in the M2 H-abstraction reaction on $Si(OH)_4$ cluster (BhandHLYP/6-311g(d,p)).

(5.91 kcal/mol) than in the gas phase (5.42 kcal/mol). This effect, of course, is mainly due to the higher energy of the pre-reactive complex. It suggests that the presence of a silicate surface may not favor the reaction. We shall see that the rate constants results agree with this conclusion.

For the M2 H-abstraction mechanism, the geometry of the transition state is different from the M1 mechanism, because the OH• radical has the possibility to interact with terminal silanol groups on the surface, thus giving rise to an unusually stable transition state (Figure 8.b). The corresponding transition vector shows the characteristic H atom motion between the C_f and O_{oh} atoms.

All stationary structures for the H-abstraction reactions are shown in Figures 6 to 8. Relative energy and Gibbs free energy values are given in Table 2. In this table, energies are calculated relative to the separated reactants (surface bound formaldehyde and a free OH• radical) and include ZPE corrections The E_{-1} energy is the pre-reactive complex stabilization energy, which is calculated as $E_{-1}=E_{RC}-E_R$; E_2 is the reaction barrier for the second step of the complex mechanism, $E_2=E_{TS}-E_{RC}$; E_a^{eff} is the effective activation energy, $E_a^{eff}=E_{TS}-E_R$; and ΔE is the reaction energy, $\Delta E=E_{products}-E_{reactants}$. The negative frequencies corresponding to the motion along the reaction path have also been indicated for the transition states in Table 2.

The results obtained for the M2 H-abstraction mechanism (Figure 8) are contradictory. On the one hand, it is clear that if silanol groups are available, formaldehyde will preferentially adsorb to form the ADS1 complex, which is considerably more stable than ADS2. In the absence of silanol groups, the formation of an ADS2 complex could be considered. We have modeled this possibility with the $Si(OH)_4$ monomer, by forcing the formaldehyde adsorption on the oxygen atoms of two silanol groups. Yet the corresponding transition state (Figure 8.b) has a very low energy, because the OH• radical interacts with a surface silanol, thus entering in contradiction with the original assumption. We shall see that the same is true for the OH• addition reaction. Thus, the M2 mechanisms are not pursued further with this model.

OH-addition Mechanism

As mentioned before, another process may also occur, which leads to OH• radical addition to the formaldehyde C=O bond. Starting from the ADS1 adsorption complex and the corresponding pre-reactive complex, two different transition states have been identified. In one of them, the radical approaches the formaldehyde carbon atom without interacting with the orthosilicic moiety (TSadd1). In the other, the radical is attracted to the oxygen atom of the same silanol group that is already involved in the formation of the hydrogen bond with formaldehyde (TSadd2). They are very different in shape, but both OH•-addition mechanisms present similar E_2 energy barriers. It is also interesting to note that, although these transition states have energies that are considerably larger than in the abstraction channel, both are smaller than in the gas phase OH•-addition pathway, and they occur slightly later than in the gas phase. The product complexes are also slightly more stable than in the gas phase.

All stationary structures are shown in Figures 10 and 11. Energy values are calculated relative to the separated reactants, and are given in Table 3, including ZPE corrections. In order to take into account the entropy changes, Gibbs free energies are also included.

Reaction Kinetics

For the formaldehyde + OH• reaction, experimental results are only available in the gas phase. Thus, this value is used to validate the methodology employed. The energy values, partition functions and thermodynamic data for the abstraction and addition reactions in the gas phase are obtained from BHandHLYP/6-311G** quantum chemistry calculations The

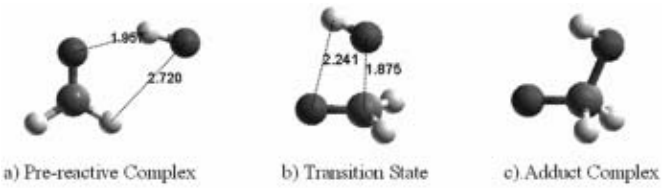

Fig. 9. Optimized structures in the gas phase addition reaction (BhandHLYP/6-311g(d,p)).

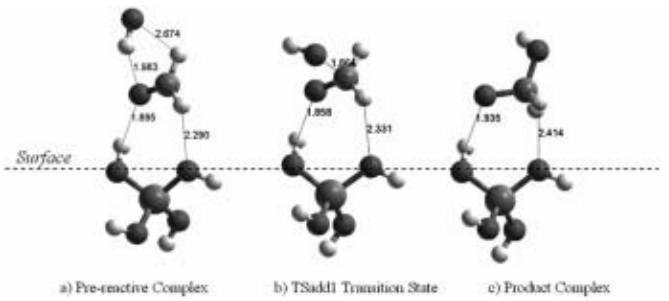

Fig. 10. Optimized structures in the OH-addition reaction on Si(OH)4, using the TSadd1 (BhandHLYP/6-311g(d,p)).

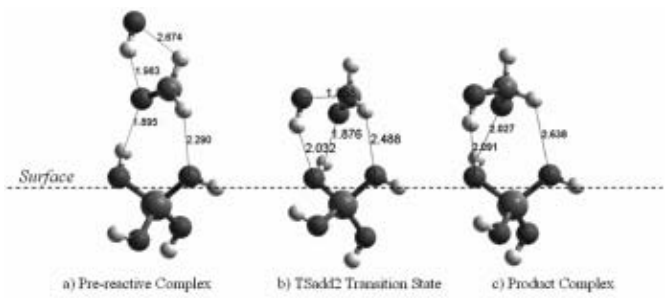

Fig. 11. Optimized structures in the OH-addition reaction on $Si(OH)_4$, using the TSadd2 (BhandHLYP/6-311g(d,p)).

rate constants are determined using Transition State Theory. In all cases the complex mechanism, Eqs. 3 and 4, has been assumed to occur.. The effective rate constant is obtained using the following equation:

$$k_{ef} = \sigma\, \kappa_2 \frac{Q^{TS}}{Q^R} \exp\left[-\frac{E_a^{eff}}{RT}\right].$$

The tunneling correction κ_2 of the second step is calculated according to the Eckart [62] model, with an asymmetric barrier. It depends on the size and shape of the E_2 barrier. The kinetic parameters are obtained from the rate constants (in cm^3 $molecule^{-1}$ s^{-1}) in the range 200 to 330 K (Table 6).

As explained in the methodology section, internal rotations with barriers smaller than 2.5 Kcal/mol have to be identified and treated as rotations in the calculation of the partition functions. In the H-abstraction transition state, only one such internal rotation occurs. It corresponds to the rotation of the OH• hydrogen atom around the H_f ••• O_{oh} axis. A plot of the electronic energy as a function of the C-H-O-H dihedral angle, obtained using the BHandHLYP/6-311(d,p) method (Figure 12) presents a maximum barrier of 2.5 kcal/mol. Thus, this motion has to be treated as an internal rotation in the calculation of the transition state partition function. The calculated total hindered rotor correction factor of the partition function at 298 K, however, is found to be quite small (=1.13) and therefore the effect, on the rate constant, of introducing the correction for this internal rotation, is well within the range of the experimental error. In the case of the addition pathway, this correction is not necessary because its transition state structure does not present internal rotations.

The results obtained for the gas phase formaldehyde + OH• reaction, using the above methodology, are shown in

Table 2. Relative Energies (including ZPE) in kcal/mol, and imaginary frequencies (υ_i) at the transition states (in cm^{-1}), in the H-abstraction reaction. In this table, $E_{-1}=E_{RC}-E_R$; $E_2=E_{TS}-E_{RC}$; $E_a^{eff}=E_{TS}-E_R$; and $\Delta E=E_{products}-E_{reactants}$.

*BHandHLYP/6-311g***	$E_{adsorption}$	E_{-1}	E_{-2}	E_a^{eff}	ΔE	ΔG	υ_i
Gas phase H-abstraction	-	-5.19	5.42	0.24	-22.56	-23.00	-932
$Si(OH)_4$ M1 H-abstraction	-7.37	-4.96	5.91	0.95	-20.15	-21.01	-1204
$Si(OH)_4$ M2 H-abstraction	-1.96	-5.32	0.83	-4.49	-30.39	-21.16	-356
CBS-QB3	$E_{adsorption}$	E_{-1}	E_{-2}	E_a^{eff}	ΔE	ΔG	υ_i
Gas phase H-abstraction	-	-3.30	2.47	-0.83	-30.35	-30.81	-183
$Si(OH)_4$ M1 H-abstraction	-5.52	-3.06	2.16	-0.90	-28.25	-29.10	-107

Table 3. Relative Energies (including ZPE) in kcal/mol, and imaginary frequencies (υ_i) at the transition states (in cm^{-1}), of the OH radical addition reaction.

*BHandHLYP/6-311g***	E_{-1}	E_{-2}	Ea^{eff}	ΔE	ΔG	υ_i
Gas phase OH-addition	-5.20	11.14	5.94	-22.99	-14.69	-556
$Si(OH)_4$ OH-addition (TSadd1)	-5.96	10.78	5.82	-22.05	-13.68	-542
$Si(OH)_4$ OH-addition (TSadd2)	-5.96	9.12	4.16	-23.27	-14.28	-567

Table 4. Calculated rate constants (in cm^3/molecule s) at 298 K for the H-abstraction reactions.

BHandHLYP/6-311g**	σ	K_{eq}	κ	k_2	k^{ef}	k^{exp}
Gas phase H-abstraction	2	9.68×10^{-22}	2.71	1.14×10^{10}	1.10×10^{-11}	1.0×10^{-11}
M1 H-abstraction	1	8.25×10^{-22}	5.00	1.95×10^{9}	1.61×10^{-12}	-
CBS-QB3	σ	K_{eq}	κ	k_2	k^{ef}	k^{exp}
Gas phase H-abstraction	2	2.23×10^{-22}	1.12	6.43×10^{10}	1.43×10^{-11}	1.0×10^{-11}
M1 H-abstraction	1	5.73×10^{-23}	1.06	8.29×10^{10}	4.74×10^{-12}	-

*Experimental result from Reference 12

Tables 4 and 5. At 298K, the recommended value is $k_{298} = 1.0 \times 10^{-11}$ cm^3 $molecule^{-1}$ s^{-1} [12], with an uncertainty factor f(298) of 1.25. Thus, our calculated results are in excellent agreement with the experimental value at this temperature, and within the range of the experimental error. It can be seen that, at 298ºK the addition channel is negligible, and that the calculated abstraction rate constant agrees very well with the experimental results. Thus, the same methodology will be used next for the OH• reaction with adsorbed formaldehyde.

Table 5. Calculated rate constants (in cm^3/molecule s) at 298 K for the OH-addition channels.

BHandHLYP/6-311g**	σ	$k_{forward}$
Gas phase OH-addition	1	1.61×10^{-17}
M1 OH-addition (TSadd1)	1	0.94×10^{-17}
M1 OH-addition (TSadd2)	1	2.07×10^{-17}

Table 6. Arrhenius parameters in the range 200 - 330 K.
$k(T) = AT^n\exp[-E_a/RT]$

	A	*n*	*Ea/R*
H-abstraction TST	5.35×10^{9}	1.19	2.80×10^{3}
H-abstraction TST/Eckart	3.43×10^{5}	2.28	1.29×10^{3}
OH-addition TST	3.15×10^{11}	-0.82	3.08×10^{3}

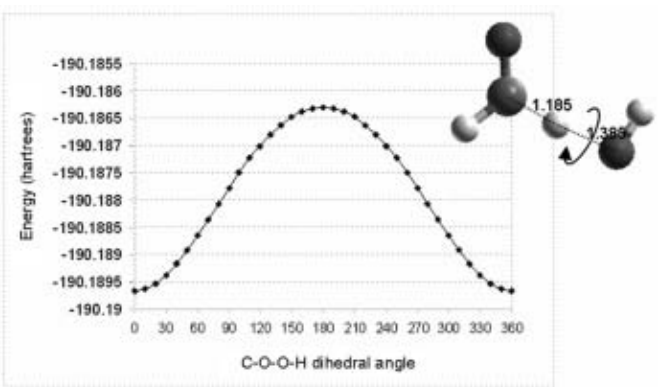

Fig. 12. Plot of the electronic energy as a function of the C-H-O-H dihedral angle (BHandHLYP/6-311g**).

As explained earlier, rate constants have been calculated only for the ADS1 complexes because the M2 mechanism leads to structures that are stabilized by interactions with silanol groups, in contradiction with the assumption that ADS2 complexes can exist only in the *absence* of these groups. For the M1 H-abstraction reaction, only one internal rotation has to be taken into account. As in the gas phase, the latter corresponds to the rotation of the OH hydrogen atom around the Cf-Hf---Or axis. The rotation barrier is 2.1 kcal/mol, and the corresponding partition function correction factor is 1.07. A plot of the energy as a function of the C-H-O-H dihedral angle is shown in Figure 13. The calculated rate constant is *smaller* (1.61×10^{-12} cm^3 $molecule^{-1}$ s^{-1}) than in the gas phase reaction (1.10×10^{-11} cm^3 $molecule^{-1}$ s^{-1}), in agreement with the fact that its effective activation energy is larger than in the gas phase. In this mechanism, the reaction symmetry number is equal to one, because only one formaldehyde hydrogen can be abstracted. On the other hand, a lower reactivity of the adsorbed formaldehyde is in line with the effect of the less stable pre-reactive complex.

For the M1 OH-addition mechanisms, one of the calculated rate constants (TSadd1) is found to be slightly *smaller* than in the gas phase addition, while in the case of the bound-OH-addition channel (TSadd2), the rate constant is slightly *larger* than in the gas phase. The overall rate constant, which measures the rate of OH• disappearance [63], can be determined as the sum of the rate coefficients calculated for the different pathways. However, rate coefficients corresponding to the addition mechanism are so much smaller than those of the abstraction channel, that their contribution is negligible.

Arrhenius plots of the M1 H-abstraction and OH-addition rate constants are shown in Figures 14 and 15, and both exhibit some temperature dependence. For the M1 H-abstraction, the calculated overall rate constant in cm^3 $molecule^{-1}$ s^{-1} is given by the expression $k^{eff} = 3.43 \times 10^5 T^{2.28}\exp(-2.57/RT)$. In the same units, the rate constant for the M1 OH-addition mechanism is $k^{ef} = 3.15 \times 10^{11} T^{-0.82}\exp(-6.16/RT)$.

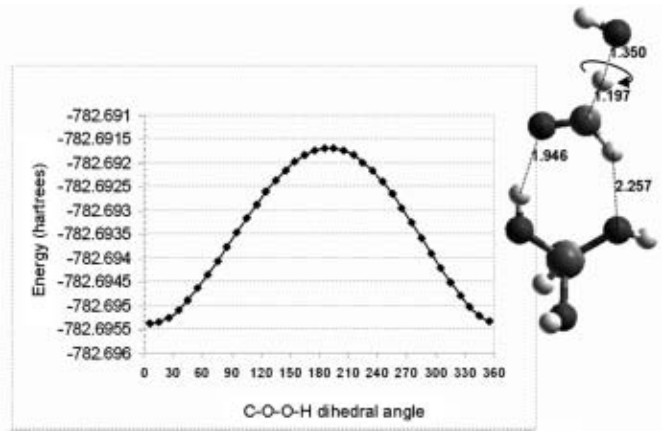

Fig. 13. Plot of the electronic energy as a function of the C-H-O-H dihedral angle (BHandHLYP/6-311g**)

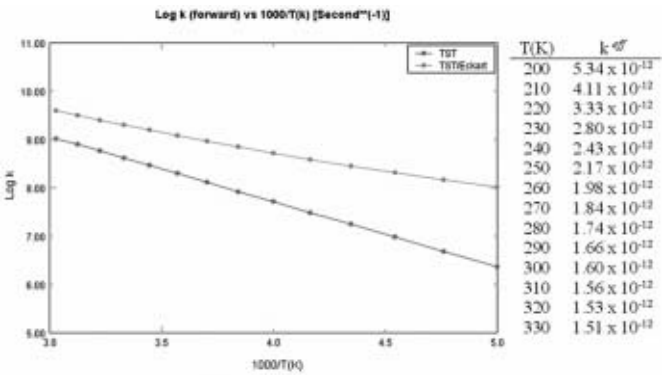

Fig. 14. Arrhenius plot of the k_2 rate constants for the M1 H-abstraction pathway, in the range 200-330 K.

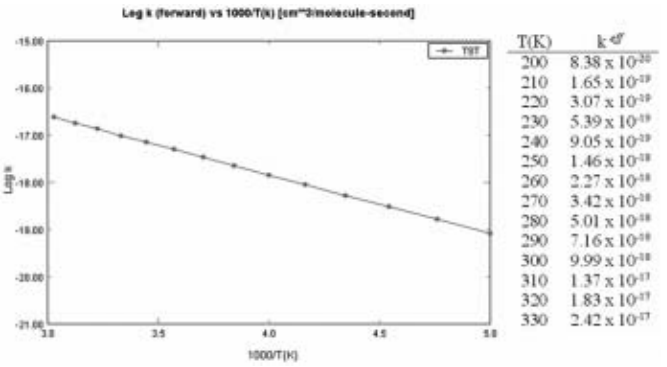

Fig. 15. Arrhenius plot of the direct rate constants for the M1 H-addition pathway, in the range 200-330 K.

For the abstraction channel, it is important to note that, in the particular case of a reaction involving the migration of a hydrogen atom, the tunneling factor is important, affecting the calculation of the rate constant. However, in the case of the addition channel, no tunneling effect is expected to occur.

Conclusions

In this work, the mechanism of the reaction between an OH• radical and a formaldehyde molecule attached to a $Si(OH)_4$ silicate cluster model has been studied with the BHandHLYP/6-311G** and CBS-QB3 quantum chemistry methods. The adsorption of formaldehyde was investigated in all possible manners, considering that formaldehyde interacts with the surface atoms either using its oxygen and one hydrogen atom (forming the ADS1-type adsorption complex), or through both hydrogen atoms (ADS2). Since natural clays present numerous fractures and, in general, silanol groups are available, one can expect that adsorption of formaldehyde will normally occur in their vicinity and form ADS1-type complexes, which are about 5 kcal/mol more stable than ADS2.

The potential energy surfaces for the bound formaldehyde reaction with OH• radicals were carefully spanned, considering both adsorption complexes. For each of them, H-abstraction and OH• addition reactions were investigated. These are complex reactions that involve the formation of a reactant complex in the entrance channel and a product complex in the exit channel.

The reaction of OH• with the ADS2 adsorption complex leads to transition states and products in which the OH• radical invariably attaches to an orthosilicic silanol group, thus contradicting the original premise that ADS2 is formed when no OH• groups are available on the surface. For this reason, we consider that this model is not appropriate for the representation of the reaction in the absence of surface silanol groups.

The activation energy for addition of the OH• radical to the double bond of adsorbed formaldehyde is found to be similar to the gas phase value and much higher than the one for hydrogen abstraction. The corresponding rate constants are five orders of magnitude smaller than for H-abstraction.

On the basis of the calculated rate constants we conclude that, when the OH•-formaldehyde reaction occurs in the presence of dust, at atmospheric pressure, it is *slower*, by a factor of about ten, than the reaction in the gas phase. If one takes into account the fact that silicate aerosols are known to trap some of the OH• radicals in the troposphere, the resulting decrease in the formaldehyde reaction rate with OH• could be significant.

Acknowledgments

The authors are grateful to CONACYT Project No. SEP-2004-C01-46167-Q and to the PIFI 3.3 program for financial support. We also thank Professors W. T. Duncan, R. L. Bell and T. N. Truong for providing the Rate program through Internet.

References

1. Usher, C. R.; Michel, A. E.; Grassian, V. H. *Chem. Rev.* **2003,** 103, 4883-4939.
2. Dentener, F. J.; Carmichael G. R.; Zhang Y. *J. Geophys. Res.* **1996**, 101, 22869–22889.

3. Bian, H. S.; Zender, C. S**.** *J. Geophys. Res.* **2003**, 108, 4672.
4. Ravishankara, A. R. *Science* **1997**, 276, 1052-1058.
5. S. Oh; J. M. Andino *Atm. Environ.* **2002**, 36, 149-156.
6. M. Sørensen; M. D. Hurley; T. J. Wallington; T. S. Dibble; O. J. Nielsen. *Atm. Environ.* **2002**, 36, 5947-5952.
7. Carlos-Cuellar, S.; Li, P.; Christensen, A. P.; Krueger, B. J.; Burrichter, C.; Grassian, V. H. *J. Phys. Chem. A* **2003**, 107, 4250-4261.
8. Atkinson, R. *J. Phys. Chem. Ref. Data* **1994**, Monograph 2, 1.
9. Tyndall, G. S.; Orlando, J. J.; Wallington, T.; Hurley, M. D.; Goto, M.; Kawasaki, M. *Phys. Chem. Chem. Phys.* **2002**, *4*, 2189-2193.
10. Vandenberk, S.; Peeters, J. *J. Photochem. Photobiol. A* **2003**, *157*, 269-274.
11. Atkinson, R.; Baulch, D. L.; Cox, R. A.; Hampson, R. F., Jr.; Kerr, J. A.; Rossi, M. J.; Troe, J. *J. Phys. Chem. Ref. Data* **1997**, *26*, 521-1011.
12. DeMore, W. B.; Sander, S. P.; Golden, D. M.; Hampson, R. F.; Kurylo, M. J.; Howard, C. J.; Ravishankara, A. R.; Kolb, C. E.; Molina, M. J., JPL-PUBL-92-20; NAS 1.26192795; NASA-CR-192795.
13 Alvarez-Idaboy, J. R.; Mora-Diez, N.; Boyd, R. J.; Vivier-Bunge, A. *J. Am. Chem. Soc*. **2001**, 123, 2018-2024.
14 Aloisio, S.; Francisco, J. S. *J. Phys. Chem. A* **2000**, 104, 3211-3224.
15 Gutmann, V. In The *Donor-Acceptor Approach to Molecular 1nteractions;* Plenum Press, New York, **1978**.
16 Gutmann, V.; Resch, G.; Linert, W. *Coord. Chem. Rev.* **1982**, 43, 133-164.
17. Bronnimann. C. E.; Zeigler, R. C.; Maciel, *G.* E. *J. Am. Chem. Soc.* **1988**, *110*, 2023-2026.
18. Morrow. B. A.; Gay, I. D. *J. Phys. Chem.* **1988**, 92, 5569-5571.
19. Legrand, A. P.; Hommel, H.; Taibi, H.; Miquel, J. L.; Tougne, P. *Colloid Surf.* **1990**, 45, 391-411.
20. Leonardelli. S.; Facchini, L.; Fretigny, C.; Tougne. P.; Legrand, A. P. *J. Am. Chem. Soc.* **1992**, 114, 6412-6418.
21. Hoffman, P.; Knozinger, E. *Surface Sci.* **1987**, 188, 181-198.
22. McFarlan, A. J.; Morrow, B. A. *J. Phys. Chem.* **1991**, 95, 5388-5390.
23. Knozinger, H. In *The hydrogen bond*, Vol. 111, Schuster, P.; Zundel, *G.;* Sandorfy, C., Eds., North-Holland: Amsterdam **1976**; 1263, and references therein.
24. Her, R. K. In *The chemistry of silica;* Wiley-Interscience: New York **1979**; Chapter 6.
25. Kiselev, A. V.; Lygin, V. I. In *lnfrared spectra of surface compounds;* Wiley: New York, **1975**.
26. Heanry, P. J.; Prewitt, C. T.; Gibbs, G. V. In *Silica, Physical Behavior, Geochemistry and Materials Applications*; Ribbe, P. H., Ed.; *Reviews in Mineralogy*, Vol. 29; Mineralogical Society of America: Washington, D.C., **1994**; 331.
27 Sauer, J.; Ugliengo, P.; Garrone, E.; Saunders, V.R. *Chem. Rev.* **1994**, 94, 2095-2160.
28. Xin, L.; Qianer, Z.; Lin, M. C. *Phys. Chem. Chem. Phys*. **2001**, 3, 2156-2161.
29.Sauer, J.; Ugliengo, P.; Garrone, E.; Saunders, V. R. *Chem. Rev.* **1994**, 94, 2095-2160.
30. Ugliengo, P**.;** Saunders, V. R.; Garrone, E. *Chem. Phys. Lett.* **1990,** 169, 501-508.
31. Busca, G.; Lamotte, J.; Lavalley, J. C.; Lorenzelli, V. *J. Am. Chem. Soc.* **1987**, 109, 5197-5202.
32. Sauer, J.; Schrader, K. P. *Phys. Chem. Leipzig* **1985**, 266, 379.
33. Pelmenschikov, A. G.; Morosi, G.; Gamba, A. *J. Phys. Chem.* **1992**, 96,7422-7424.
34. Sauer, J. *J. Phys. Chem.* **1987**, 91, 2315-2319.
35. Ugliengo, P.; Garrone, E., *J. Mol. Catal.* **1989**, 54, 439-443.
36. Ugliengo, P.; Saunders, **V.** R.; Garrone, E. *J. Phys. Chem.* **1989**, 93, 521.
37. Garrone, E.; Ugliengo, P. *Mater Chem. Phys.* **1991**, 29, 287-296.
38 Civalleri, B.; Garrone, E.; Ugliengo, P. *Chem. Phys. Lett.* **1998**, 294, 103-108.
39 Pereira, J. C. G.; Catlow, C. R. A.; Price, G. D. *J. Phys. Chem. A* **1999**, *103*, 3268-3284.
40. Becke, A. D. *J. Chem. Phys.* **1993**, 98, 1372-1377.
41. Raghavachari, K.; Foresman, J. B.; Cioslowski, J.; Ortiz, J. V.; Frisch, M. J.; Frisch, A. *GAUSSIAN 98 User's Reference*; Gaussian Inc.: Pittsburgh, PA, **1998**.
42. Gaussian 03 (Revision A.1), Frisch, M. J.; Trucks, G. W.; Schlegel, H. B.; Scuseria, G. E.; Robb, M. A.; Cheeseman, J. R.; Montgomery, J. A. Jr.; Vreven, T.; Kudin, K. N.; Burant, J. C.; Millam, J. M.; Iyengar, S. S.; Tomasi, J.; Barone, V.; Mennucci, B.; Cossi, M.; Scalmani, G.; Rega, N.; Petersson, G. A.; Nakatsuji, H.; Hada, M.; Ehara, M.; Toyota, K.; Fukuda, R.; Hasegawa, J.; Ishida, M.; Nakajima, T.; Honda, Y.; Kitao, O.; Nakai, H.; Klene, M.; Li, X.; Knox, J. E.; Hratchian, H. P.; Cross, J. B.; Adamo, C.; Jaramillo, J.; Gomperts, R.; Stratmann, R. E.; Yazyev, O.; Austin, A. J.; Cammi, R.; Pomelli, C.; Ochterski, J. W.; Ayala, P. Y.; Morokuma, K.; Voth, G. A.; Salvador, P.; Dannenberg, J. J.; Zakrzewski, V. G.; Dapprich, S.; Daniels, A. D.; Strain, M. C.; Farkas, O.; Malick, D. K.; Rabuck, A. D.; Raghavachari, K.; Foresman, J. B.; Ortiz, J. V.; Cui, Q.; Baboul, A. G.; Clifford, S.; Cioslowski, J.; Stefanov, B. B.; Liu, G.; Liashenko, A.; Piskorz, P.; Komaromi, I.; Martin, R. L.; Fox, D. J., Keith, T.; Al-Laham, M. A.; Peng, C. Y.; Nanayakkara, A.; Challacombe, M.; Gill, P. M. W.; Johnson, B.; Chen, W.; Wong, M. W.; Gonzalez, C.; Pople, J. A.; Gaussian, Inc., Pittsburgh, PA, **2004**.
43. Galano, A.; Alvarez-Idaboy, J. R.; Ruiz-Santoyo M. E.; Vivier-Bunge, A. *J. Phys. Chem. A* **2002**, 106, 9520-9528.
44. Galano, A.; Alvarez-Idaboy, J. R.; Bravo-Pérez G.; Ruiz-Santoyo, M. E., *Phys. Chem. Chem. Phys.* **2002**, 4, 4648–4662.
45. Mayer, I. *Int. J. Quantum. Chem.* **1983**, 23, 341-363.
46. Mayer, I. *J. Phys. Chem.* **1996**, 100, 6332-6335.
47. Frisch, M. J.; Del Bene, J. E.; Binkley, J. S.; Schaefer III, H. F.; *J. Chem. Phys*. **1986**, 84, 2279-2289.
48. Schwenke, D. W.; Truhlar, D. G. *J. Chem. Phys*. **1985**, 82, 2418-2426.
49 T. H. Dunning, Jr. *J. Phys. Chem. A* **2000**, 104, 9062-9080..
50. Eyring, H., *J. Chem. Phys.*, **1935**, 3, 107-115.
51. Truhlar, D. G.; Hase W. L.; Hynes, J. T., *J. Phys. Chem.*, **1983**, 87, 2264-2267.
52. Duncan, W. T.; Bell, R. L.; Truong, T. N., *J. Comput. Chem.* **1998**, 19, 1039-1052.
53. Singleton, D. L.; Cvetanovic, R. J., *J. Am. Chem. Soc*. **1976**, 98, 6812-6819.
54. Pilling, M. J.; Seakins, P. W. *Reaction Kinetics*, Oxford University Press, New York, **1996**.
55. Laidler, K. J., Chemical Kinetics, ed. Harper Collins Publishers, **1987**, p. 98.
56. Jacox, M. E. *Vibrational and Electronic Energy Levels of Polyatomic Transient Molecules*, Vol. 69, NIST: Gaithersburg, MD, **1998**, 945.
57 The NIST Chemical Kinetics Data Base, NIST Standard Reference Database; U.S. Dept. of Commerce, Technology Administration, National Institute of Standards and Technology: Gaithersburg, MD, 17-2Q98.
58. Guggenheim, S.; Chang, Y.-H.; Koster van Gross, A.F. *American Mineralogist*, **1987,** 72, 537-550.
59. Lee, J. H.; Guggenheim S. *American Mineralogist*, **1981**, 66, 350-357.
60. Knozinger, H. In *The Hydrogen Bond*; Vol III, Schuster, P., Zundel, G., Sandorfy, C., Eds.; North-Holland: Amsterdam, **1976**, 1263; and reference therein.
61. Curthoys, G.; Davydov, V. Ya; Kiselev, A. V.; Kiselev, S. A.; Kuznetsov, B. V. *J. Colloid Interface Sci.* **1974**, *48*, 58-72.
62. Truong, T. N.; Truhlar, D. G. *J. Chem. Phys.* **1990**, 93, 1761-1769.
63. Tiee, J. J.; Wampler, F. B.; Oldenborg, R. C.; Rice, W. W. *Chem. Phys. Lett.* **1981**, 82, 80-84.